NASA Technical Paper 2488

July 1985

Surface Roughness Effects in Elastohydrodynamic Contacts

John H. Tripp and
Bernard J. Hamrock

NASA

NASA Technical Paper 2488

1985

Surface Roughness Effects in Elastohydrodynamic Contacts

John H. Tripp and
Bernard J. Hamrock

Lewis Research Center
Cleveland, Ohio

National Aeronautics
and Space Administration

**Scientific and Technical
Information Branch**

Summary

Theoretical studies of surface roughness effects in full-film EHL contacts are described. The analysis, using a flow factor modification to the Reynolds equation, was applied to piezoviscous-elastic line contacts. Carefully converged results for ensemble-averaged film shape, pressure distribution, and other mechanical quantities were obtained. Asperities elongated in the flow direction by a factor exceeding 2 decreased both film shape and pressure extrema at constant load; isotropic or transverse asperities increased these extrema. Changes were small, of order 1 percent, and the EHL spike showed no special sensitivity. The largest effects were displayed by traction, which increased by over 5 percent for isotropic or transverse asperities and by slightly less for longitudinal roughness.

Introduction

The conventional elastohydrodynamic model of concentrated lubricated contacts is based on laminar flow of a Newtonian fluid between smooth, elastic bounding surfaces. The physical basis for this model, developed over the last 25 years or so, has been amply reviewed in the recent book of Hamrock and Dowson (ref. 1), where details of actual calculations and applications are given. With this understanding extensions of the fundamental model to include additional effects, such as nonlaminar flow, non-Newtonian rheology, or thermal behavior are feasible. The present work describes theoretical studies of some of the effects of surface roughness on the lubricant film, where a random texture was superimposed on the smooth, nominal film shape representative of the kinds of surface finish found in engineering practice. This work is particularly concerned with the random aspect of surface asperities. Once the local film thickness h becomes a stochastic variable, model solutions are possible only in a statistical sense, and at some point an ensemble averaging must be performed. Previous attempts to develop equations capable of handling roughness effects have been critically reviewed by Elrod (refs. 2 and 3), who notes that most early treatments were restricted to one-dimensional roughness textures, or striations, parallel to which the film profile remained smooth. One approach to the problem of two-dimensional surface roughness is to derive a modified Reynolds equation in which h and the pressure p are replaced by their ensemble-averaged values. Such an approach is justified to some extent since the appearance of h in the Reynolds equation is itself only the result of applying a boundary condition on the Navier-Stokes equation at the true surface. Its validity is, however, limited to surface textures that do not destroy the laminar flow of the film, and this sets a lower limit to the roughness correlation lengths measured in terms of h. Elrod (ref. 3) suggests $5h$ as a suitable value. The validity of the Reynolds equation also depends on roughness heights being small, since otherwise pressure and velocity begin to vary across the film. In combination these two conditions amount to an average slope limitation distinguishing between the regimes of Reynolds and Stokes roughness.

Of the many ways to derive new Reynolds equations, those emphasizing the conservative nature of the lubricant flow seem most appropriate (refs. 3 and 4). Such flow methods recognize that although h and p are local fluctuating quantities, they are also correlated since the flow described by their products and derivatives fluctuates only on a global scale. Thus, if h and p are replaced in the Reynolds equation by their average values, the effects of this correlation can be adequately described by a set of flow factors appearing in the modified Reynolds equation. These flow factors represent various lubricant entrainment effects of the surface texture and, provided that flow fluctuations are ignored entirely, are deterministic properties of the surfaces and the nominal film thickness. A calculation of these tensor flow factors by a perturbation expansion in powers of $1/\Lambda$, where Λ is the film parameter, has been described elsewhere (ref. 5) in a paper referred to herein as I.

The final structure of the modified Reynolds equation was only slightly more complex than the original smooth-surface form: for the case considered of a line contact in pure rolling with incompressible lubricant, no additional terms were involved. The constant fluid density, however, was replaced by the flow factors. Consequently, computational methods described in the recent work of Hamrock and Jacobson (ref. 6), referred to herein as II, were readily adapted to the study of roughness effects on

the EHL of line contacts. Although the methods are similar, EHL calculations are notoriously sensitive to changes in lubricant behavior, and the roughness, acting as an effective compressibility dependent on h rather than p, has a marked effect on the convergence of the solution. Following a brief summary of the formalisms reduced from I and II, some of the peculiarities of the solution procedure required by the presence of the flow factors are discussed.

To the lowest nonvanishing order of perturbation theory, roughness effects are determined by just two parameters. The rms surface height σ referenced to h defines the first parameter, which in the usual notation becomes the film parameter $\Lambda = h/\sigma$. The second parameter describes the anisotropy of typical surface asperities given by γ, the ratio of the two-point correlation lengths parallel and perpendicular to the lay direction of the surface texture. For conditions typical of an EHL contact in the piezoviscous-elastic regime with a well-developed pressure spike near the outlet, the film shape was calculated as a function of γ and Λ_{m0}, where the double subscript indicates that σ is normalized to the value of the minimum film thickness $h_{m,0}$ for the contact operating with a smooth surface: $\Lambda_{m,0} = h_{m,0}/\sigma$. Other mechanical quantities associated with the contact have been computed, and typical results for the traction coefficient are presented.

Symbols

This symbol list includes definitions of some of the variables needed later in the formalism. The configuration to be described (fig. 1) consists of two rough, elastic cylinders separated by a Newtonian lubricant film and rotating about axes along the y direction (perpendicular to the page).

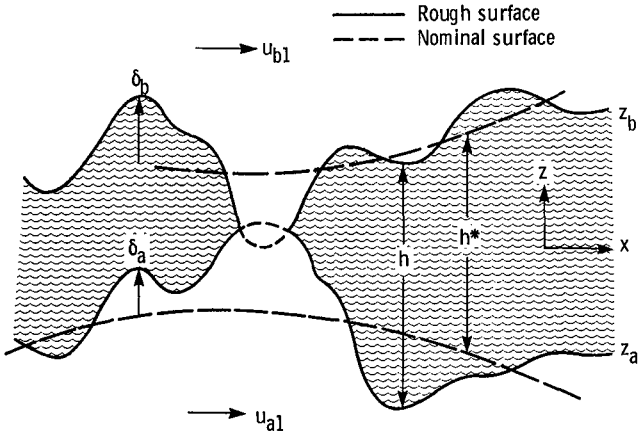

Figure 1.—Variables used in describing fluid/solid boundary in lubrication of moving rough surfaces.

b semiwidth of Hertzian contact, $R\sqrt{8W/\pi}$, m

E Young's modulus of elasticity, Pa

E' effective plane strain elastic modulus for two contacting solids, $2\left[\frac{1-\nu_a^2}{E_a}+\frac{1-\nu_b^2}{E_b}\right]^{-1}$, Pa

f force due to shear stress on surface, N/m

G dimensionless materials parameter, $1/Q_\infty$

H dimensionless nominal film thickness, h^*/R

h film thickness, $z_b - z_a$, m

K dimensionless volume flow per unit length, k/uR

k volume flow per unit length, m^2/s

P dimensionless nominal pressure, p^*/E'

p film pressure, Pa

p_{max} Hertzian maximum pressure, $2w/\pi b$, Pa

Q dimensionless isoviscous (reduced) pressure (eq. (14))

Q_∞ dimensionless asymptotic reduced pressure

R reduced radius of roller pair, $(r_a^{-1}+r_b^{-1})^{-1}$, m

r radius of roller, m

S nominal dimensionless separation of undeformed roller pair touching at origin, $x^2/2R^2$

t time, s

U dimensionless entrainment velocity, $\eta_0 u/E'R$

u_{ai} surface velocity component i of roller a, m/s

u_i mean (entrainment) velocity component i, $(u_{bi}+u_{ai})/2$, m/s

v_i slip velocity component i, $u_{bi}-u_{ai}$, m/s

W dimensionless load per unit length, $w/E'R$

w load (in z direction) per unit length, N/m

w_x x component of force due to normal stress on surface, N/m

X dimensionless coordinate, x/b

x,y,z Cartesian coordinates, m

Z Roelands viscosity-pressure exponent (eq. (16))

z mean height, $(z_b+z_a)/2$, m

z_a height of surface a, m

α viscosity-pressure index, $(\ln \eta)/p$, $(Pa)^{-1}$

γ pressure parameter in Roelands model (eq. (16)), Pa; roughness anisotropy index

Δ dimensionless elastic deformation of roller pair subject to film pressure (eq. (12))

δ_a random roughness height of surface a, $z_a - z_a^*$, m

δ_{ij} Kronecker delta, 2×2 unit matrix

ζ relative contribution of pressure gradient to flow (eq. (7))

η lubricant viscosity, Pa s

$\bar{\eta}$ dimensionless viscosity, η/η_0

η_0 viscosity at ambient pressure, Pa s

η_1 viscosity parameter in Roelands model (eq. (16)), Pa s

Λ dimensionless film parameter, h^*/σ

μ coefficient of rolling friction; traction coefficient

ν Poisson's ratio

σ rms value of $\delta_b - \delta_a$, equal to $(\sigma_b^2 + \sigma_a^2)^{1/2}$ if a,b are uncorrelated, m

φ_{ij}^p pressure flow factor

φ_{ij}^s shear flow factor

Subscripts:

a roller a

b roller b

i,j two-dimensional Cartesian vector suffixes; (x,y) denoted by value (1,2); implied summation on repeated indices

m absolute minimum film thickness

0 smooth surface

Operators:

$*$ ensemble average (expectation) operator for stochastic quantity

∂_i, ∂_j two-dimensional gradient operators, m^{-1}

Formalism

Flow Factor Method

In this section the modified Reynolds equation derived by the flow factor method is briefly reviewed and then incorporated into a full computational scheme for the elastohydrodynamic lubrication of line contacts. For one-dimensional flow the formalism of I becomes relatively simple.

The starting point for the flow factor method is to recast the flow vector k_i in terms of the average pressure and film thickness p^* and h^*, which replace their true fluctuating values p and h. To achieve this, the effects of roughness must be included explicitly. For incompressible laminar flow we have adopted the form chosen by Patir and Cheng (ref. 4):

$$k_i = -\frac{(h^*)^3}{12\eta}\varphi_{ij}^p \partial_j p^* + h^* u_i - \frac{\sigma}{2}\varphi_{ij}^s v_j \tag{1}$$

The shear flow factor φ_{ij}^s accounts for flow produced by roughness in the presence of slip even when the pressure gradient vanishes. Additional entrainment due to roughness under pure rolling conditions is included in the pressure flow factor φ_{ij}^p. Fluctuations in flow are not fully incorporated into the φ factors, but it is central to the method to assume that these fluctuations are negligible compared with those of p and h. With this assumption the continuity conditions $\partial_i k_i = -\partial h/\partial t$ can be applied to k_i^* instead of k_i, yielding the result

$$\partial_i\left(\varphi_{ij}^{p^*}\frac{(h^*)^3}{12\eta}\partial_j p^*\right) = -v_j\partial_i\left(z\delta_{ij} + \frac{1}{2}\sigma\varphi_{ij}^{s^*}\right) \tag{2}$$

where $\partial_i z$ is the mean gradient of the bounding surfaces with respect to the x,y plane. This is the modified Reynolds equation for surfaces in translational motion as given in I, where it was used to find the flow factors themselves in terms of the film parameter Λ and the anisotropy index γ.

The flow factors are locally deterministic, and a second-order perturbation calculation using Gaussian forms both for the height distribution and the two-point autocorrelation function yielded the result

$$\left.\begin{aligned}
\varphi_{11}^{p^*}(\Lambda,\gamma) &= 1 + 3\frac{\gamma-2}{\gamma+1}\Lambda^{-2} \\
\varphi_{22}^{p^*}(\Lambda,\gamma) &= \varphi_{11}^{p^*}\left(\Lambda,\frac{1}{\gamma}\right) \\
\varphi_{11}^{s^*}(\Lambda,\gamma) &= \frac{3}{\gamma+1}\Lambda^{-1} \\
\varphi_{22}^{s^*}(\Lambda,\gamma) &= \varphi_{11}^{s^*}\left(\Lambda,\frac{1}{\gamma}\right)
\end{aligned}\right\} \tag{3}$$

with all other components zero. These factors depend on the surface height distribution only through the rms value σ. Similarly, for given γ, the form of the correlation function has only a weak influence on the result. In this representation the x and y directions coincide with the roughness axes determined by the surface lay, from which the general case is readily obtained by coordinate rotation.

The forms given by equation (3) are compared in I with those computed directly from an ensemble of generated rough surfaces (refs. 4 and 7) with generally good agreement (fig. 2) in the physically realistic range of Λ. This is the full-film regime, where $\Lambda > 3$. Asperity contact, neglected in I, becomes important for smaller values, and the partial lubrication regime is generally taken to be $1 < \Lambda < 3$. By modifying the film shape near asperity contacts to allow for nonoverlap of the surfaces, the work of Bush and Hughes (ref. 8) extends the range of validity of the flow factor approach to Λ values in this range.

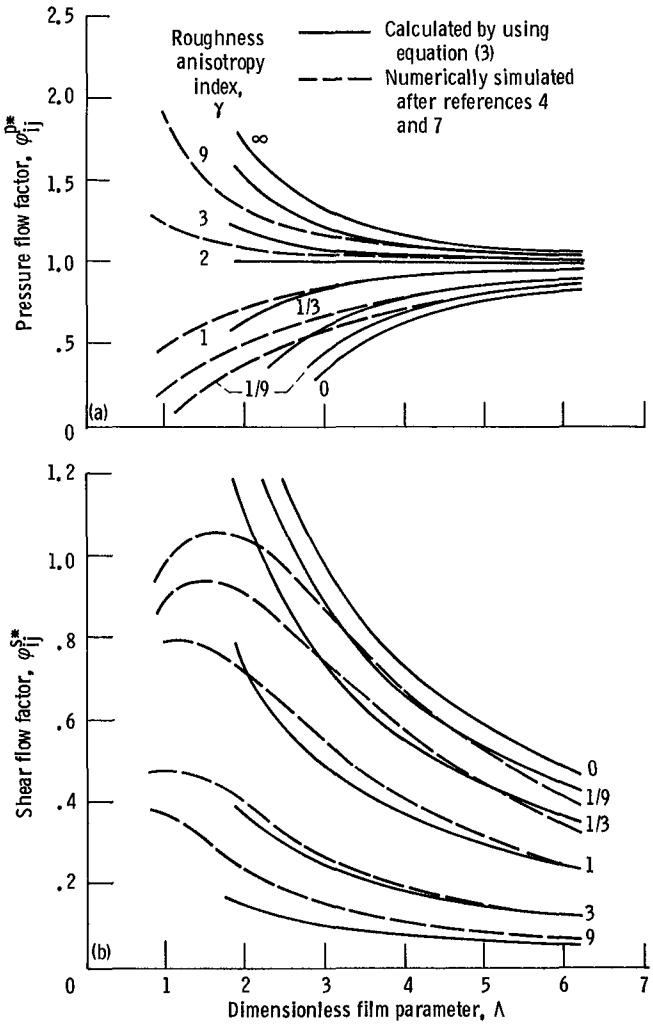

Figure 2.—Pressure and shear flow factors. (From ref. 5.)

For rotational motion about fixed axes the form of the new Reynolds equation given by equation (2) requires a slight change since the term $\partial h/\partial t$ in the continuity equation is now zero. The corresponding form of equation (2) then becomes

$$\partial_i\left(\varphi_{ij}^{p*}\frac{(h^*)^3}{12\eta}\partial_j p^*\right)=u_i\partial_i h^*-\frac{1}{2}\sigma v_j\partial_i\varphi_{ij}^{s*} \tag{4}$$

For pure rolling of cylinders about axes in the y direction, side leakage (y flow) averages to zero provided that the lay is either parallel or perpendicular to the rotation axis. Choosing the latter for illustrative purposes, we find that the flow vector of equation (1) reduces to the single component

$$k=-\frac{(h^*)^3}{12\eta}\varphi_{11}^{p*}\frac{dp^*}{dx}+h^*u \tag{5}$$

where the subscripts have been dropped from k_1 and u_1. Applying continuity to equation (5) leads to the Reynolds equation appropriate to this case:

$$\frac{d}{dx}\left(\varphi_{11}^{p*}\frac{(h^*)^3}{12\eta}\frac{dp^*}{dx}\right)=u\frac{dh^*}{dx} \tag{6}$$

This equation can be compared with its smooth-surface counterpart, equation (1) of II, the starting point of the full EHL calculations for line contact. For incompressible flow the density cancels from the equation and is replaced by the pressure flow factor in the Poiseuille term only.

Equation (5) can be cast in nondimensional form by substituting the nondimensional variables defined in the symbol list, with the result

$$K=(1-\zeta)H \tag{7}$$

where

$$\zeta=\sqrt{\frac{\pi}{2W}}\frac{H^2}{24U}\frac{\varphi_{11}^{p*}}{\bar{\eta}}\frac{dP}{dX} \tag{8}$$

The ζ term is the relative pressure (or Poiseuille) contribution to flow and is directly proportional to the (1,1) component of the flow factor.

Similar nondimensionalizing of equation (6) leads to

$$\frac{d}{dX}\left(\varphi_{11}^{p*}\frac{H^3}{\bar{\eta}}\frac{dP}{dX}\right)=24U\sqrt{\frac{2W}{\pi}}\frac{dH}{dX} \tag{9}$$

which shows that film pressure dependency on H involves explicitly the two standard nondimensional groups, entrainment speed U and applied load per unit length W. Equation (9) must be solved subject to the conditions that P begins at ambient (effectively zero) at the inlet and that the Reynolds condition $P=dP/dX=0$ holds at the outlet, the cavitation boundary.

Nominal film thickness H is given by the sum

$$H=H_0+S(X)+\Delta(X) \tag{10}$$

where $S(X)$ is the undeformed shape of the gap, $\Delta(X)$ is the elastic deformation, and H_0 is a constant equal to the difference between the central film thickness and the central elastic deformation. In the present case the contact has been loaded sufficiently heavily to yield negative values for H_0. In the usual parabolic approximation for circular cylinders

$$S(X)=\frac{4W}{\pi}X^2 \tag{11}$$

The elastic displacement of the cylindrical boundary loaded by the pressure distribution P is given within the usual linear approximation by

$$\Delta(X) = -\frac{4}{\pi}\sqrt{\frac{8W}{\pi}} \int P \ln |X-X'| dX' \tag{12}$$

Equations (11) and (12) together show that the dependence of H on P involves only the dimensionless load.

Because of the importance of the pressure (and in general temperature)-dependent viscosity $\bar{\eta}$ in the EHL solution, particular care must be exercised in choosing a model. Since $\bar{\eta}$ appears only in the denominator for dP, the viscosity can always be eliminated from the Reynolds equation by introducing the isoviscous (reduced) pressure Q defined by the Weibull transformation (ref. 9):

$$dQ = \frac{dP}{\bar{\eta}} \tag{13}$$

$$Q(P) = \int^{P} \frac{dP'}{\bar{\eta}(P')} \tag{14}$$

The viscosity model then determines the relationship of Q and P. For the present isothermal treatment of EHL we have suppressed the temperature dependence of Q and $\bar{\eta}$. Typically, Q reaches a finite upper limit Q_∞ (sometimes known as $P_{iv \cdot as}$) and rises to within a few percent of Q_∞ when P reaches three or four times Q_∞. Most EHL contacts operate with Q close to this asymptotic value, which thus becomes another important EHL variable, conventionally taken as $G = 1/Q_\infty$, the materials parameter.

Taking the Barus viscosity model as an example, we have $\bar{\eta} = e^{\alpha p}$, where α is the pressure-viscosity index. Equation (14) then gives

$$Q(P) = \frac{1 - e^{-\alpha E' P}}{\alpha E'} \tag{15}$$

from which it follows that $G = \alpha E'$.

In II the Barus fluid was used and the isoviscous Reynolds equation solved for Q. Equation (15) then yielded P, as needed for computation of the elastic displacement contribution to H, thus closing the iterative $P \leftrightarrows H$ cycle. One of the biggest problems encountered in this approach is handling the constraint $Q < Q_\infty$ when solving the isoviscous Reynolds equation. Pressures near the center of the contact may easily reach 1 GPa, whereupon e^{-GP} is of order 10^{-10}. In the spike the pressure can rise to more than twice this value so that the fractional difference between Q and Q_∞ may be as little as 10^{-20}.

To avoid some of these difficulties, we have substituted the more gently varying Roelands viscosity model (ref. 10) in place of the Barus exponential, which in any case is unrealistic at such high pressures. From Roelands' extensive analysis we have

$$\bar{\eta} = \exp\left\{\left[1 - \left(1 + \frac{PE'}{\gamma}\right)^{Z}\right] \ln \frac{\eta_1}{\eta_0}\right\} \tag{16}$$

where surprisingly the parameters η_1 and γ are almost universal constants. Fluids are thus characterized by their individual Z and η_0 values. For Roelands equation the transformation between P and Q is not particularly simple in either direction, and it proves more convenient to solve equation (9) for P directly. Thus, the reduced pressure no longer enters the computation explicitly. Its asymptotic value Q_∞ is, however, needed to determine G, for which tabulations in reference 10 were used.

Once self-consistent distributions $P(X)$ and $H(X)$ satisfying Reynolds equation (9) and the elasticity equation (12) have been obtained, various other quantities of interest can be calculated, such as the mechanical force components acting on the rollers and the friction (traction) coefficient between them. For example, the shear force per unit length f on cylinder a lies approximately in the x direction and can be written

$$f_a = \int \left(\eta \frac{\partial u}{\partial z}\right)_{z=z_a} dx \tag{17}$$

Integrating the Navier-Stokes equation for dp/dx across the film shows the integrand to be equal to $-(h/2)\, dp/dx$ in the pure rolling condition. Since this is independent of z, equation (17) also gives f_b and we have

$$f_a = f_b = -\frac{1}{2} \int h \frac{dp}{dx} dx \tag{18}$$

in which the explicit appearance of η in equation (17) is now hidden. The normal pressure p acting on the two cylinders also has a net x component $w_x = w_{ax} + w_{bx}$, which can be expressed by

$$w_x = \int h \frac{dp}{dx} dx \tag{19}$$

so that $f_a = f_b = -w_x/2$. The shear and pressure forces thus balance, satisfying the equilibrium condition

$f_a+f_b+w_x=0$. The traction coefficient for either cylinder is given by

$$\mu=\frac{|f^*|}{w} \tag{20}$$

where the expectation value of the shear force is given in second-order perturbation theory by

$$f^*=-\frac{1}{2}\int h^*\frac{dp^*}{dx}\left(1-\frac{3}{\gamma+1}\Lambda^{-2}\right)dx \tag{21}$$

TABLE I.—MATERIAL AND LUBRICANT PROPERTIES

Elastic modulus of steel rollers, E, Pa	2.00×10^{11}
Poisson's ratio for steel, ν	0.3
Inlet viscosity of paraffinic lubricant, η_0, Pa s	4.11×10^{-2}
Constants in Roelands model:	
η_1, Pa s	6.31×10^{-5}
γ, Pa	1.96×10^{8}
Roelands viscosity-pressure exponent, Z	0.67
Dimensionless asymptotic reduced pressure, Q_∞	2×10^{-4}
Effective roller radius, R, m	1.11×10^{-2}
Specific loading of rollers, w, N/m	5×10^{4}
Rolling velocity, u, m/s	5.94×10^{-1}
Hertzian semiwidth, b, m	8.02×10^{-5}
Hertzian maximum pressure, p_{max}, Pa	3.97×10^{8}
Dimensionless EHL parameters:	
U	1×10^{-11}
W	2.05×10^{-5}
G	5×10^{3}

Application

The influence of U, W, and G on EHL contacts was investigated in II. Here we focus on the effect of γ and Λ contained in $\varphi_{11}^{p^*}$ and as an illustrative application have chosen the smooth-surface conditions for case 2 of II. The pressure and film shape for this case are shown in figure 3. The pressure distribution displays a maximum near the Hertzian central maximum, followed by a definite minimum just before the spike, whose height ($\sim$1 GPa) is more than double the central value. Values of the U, W, and G parameters for this case are given in table I, which also displays one set of raw mechanical data to yield these values.

Equation (3) for the pressure flow factors shows a crossover from impeded to enhanced flow as γ increases through the critical value 2. Asperities, which on average are twice as long parallel to the flow as transverse to it, have no effect on mean flow. As representative of asperities on either side of this crossover, we have examined the isotropic case, $\gamma=1$, and the case where asperities are longer in the flow direction by a factor $\gamma=3$. Early results showed that some significant departures from the smooth-surface case were present for unexpectedly large $\Lambda_{m,0}$ values, so the range was extended to about 10. At the lower end, although no longer in the physically meaningful regime, $\Lambda_{m,0}$ was taken as low as 1 to exaggerate small trends found at larger values.

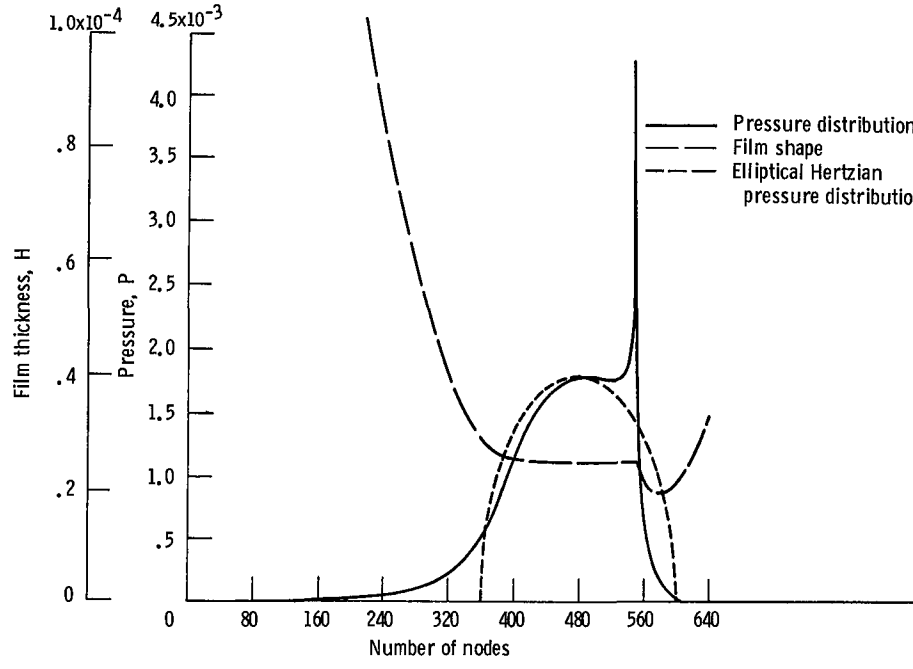

Figure 3.—Pressure distribution and film shape for an EHL contact with operating conditions $U=10^{-11}$, $W=2.05\times10^{-5}$, and $G=5\times10^{3}$. Elliptical Hertzian pressure distribution for same total load superimposed for comparison. (From ref. 6.)

Computational Method

The method is similar to that described in II and has been programmed according to the flowchart of figure 4. The equations are discretized on a uniform grid scaled to the Hertzian width and containing 660 points, with the inlet boundary condition set a distance $4b$ upstream of the contact center. The cavitation boundary floats downstream near $3b/2$. Reynolds equation (9) for P, containing the H-dependent flow factor in place of the P-dependent density, is transformed into an equation for $\Phi = PH^{3/2}$ and solved in loop 1 of figure 4 by iteration in finite difference form. The use of P rather than Q avoids problems of numerical precision arising in the transformation described by equation (14). In substituting the Roelands for the Barus fluid this transformation is not easily written in closed form. Typically, the new estimate for Φ is underrelaxed; a weight factor of 0.1 was used for the present iterate, but in difficult cases it might be as low as 0.01.

New P values for updating elastic displacements in loop 2 can likewise be weighted with previous values, but stability at this stage of the computation often permits a weight factor of 1. Elastic displacements are then computed by using the latest P by quadrature of equation (12) after analytic integration through the singularity. Loops 1 and 2 are continued until successive pressure increments fall below a chosen criterion, at which point the total load under the pressure curve must be compared with the input W value.

In loop 3a the constant H_0 of equation (10) is adjusted to bring the load into agreement with W, but even this does not produce a unique solution. Although the Reynolds equation is an expression of flow conservation, its numerical implementation by marching across the contact always from inlet to outlet allows systematic deviations from constant-flow equation (7) to appear. Such deviations must be suppressed by entering loop 3b, which again adjusts H_0. Final convergence to a unique solution is effected by passing continually between loops 3a and 3b until both load and flow conservation criteria are simultaneously satisfied. At this point calculations of force components, traction, etc., are carried out and the program terminates.

In the present computations convergence to the chosen limits proceeded more rapidly than those of II in loops 1 and 2, and in fact it was rarely necessary to iterate more than once in either loop. Moreover, no tendency for kinks to develop near the minimum of the pressure curve was encountered in loops 1 and 2 at any stage. This convenience appears to be the combined result of using Roelands viscosity and pressure P as compared with Barus and Q in II. The worst convergence problems were encountered instead in loop 3a or 3b. For example, beginning with an initial total load W in loop 3a close to the input target, the pressure curve may enter an extensive phase in which W increases with each iteration, eventually reaching some maximum value. At this point the film thickness is already too great, and it continues to rise as W returns to target from above. Generally, W now becomes too low. Once this happens, loop 3b can be activated to improve flow conservation, which continues as W passes through a minimum and approaches target from below. The entire cycle consisting of hundreds of

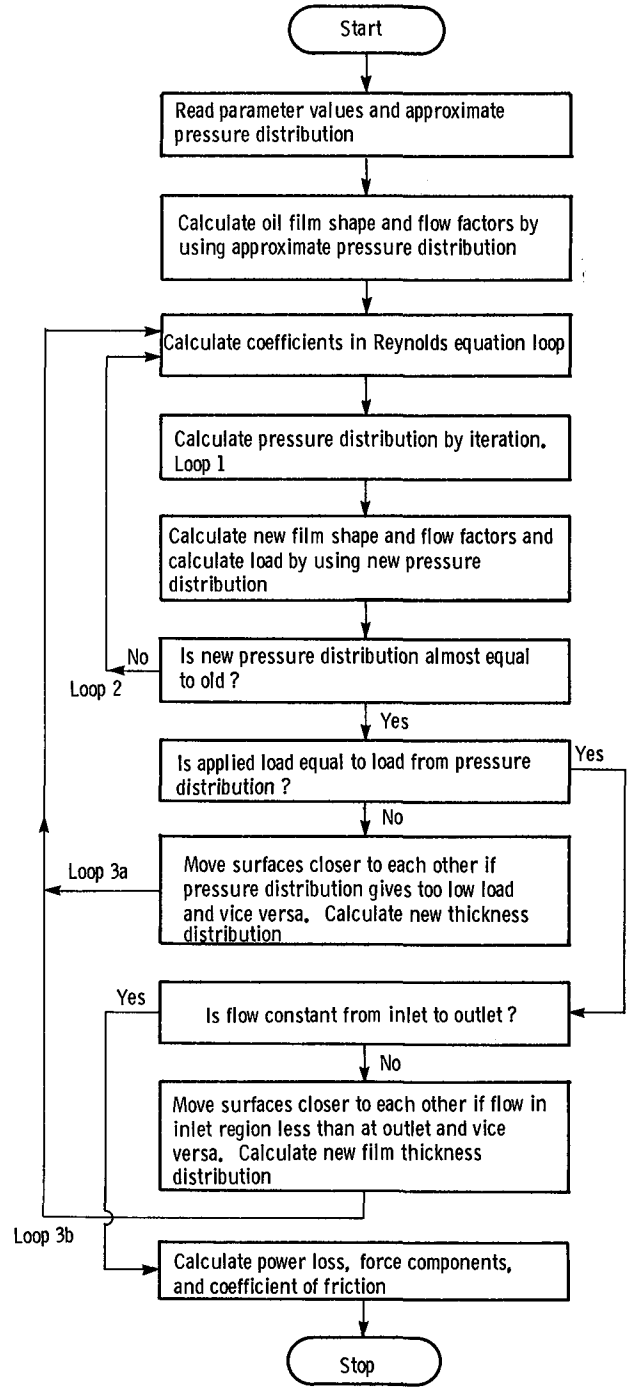

Figure 4.—Flow chart for typical EHL line contact computation.

iterations may repeat several times before both loops are converged.

The amplitude of the W swings can reach as much as 1 percent of W depending on how fast H_0 is allowed to compensate. Since this approximates the contribution to W under the sharp pressure spike, it seems likely that the inadequacy of the numerical procedure to describe this spike is an important source of load oscillations. With present grid size the width of the spike at half-peak was about 1.5 spacings so that its shape, which depends on the viscosity model, was defined by only half a dozen or so points. Shifting a spike with such sharp curvature between adjacent nodes, with no change in its true height, would produce a fluctuation in estimated load of about 0.2 percent of W. This fluctuation incidentally may be increased rather than reduced by using a higher order quadrature for W. The apparent height of the spike during such translation varies, of course, by a much larger fraction, amounting here to ~20 percent. These estimates agree with variations observed during a typical computer run, from which it is fair to assert that small movements of the pressure spike relative to the rollers is a major source of convergence difficulties. The grid at present is too coarse to allow an estimate of how much subdivision might be needed to give a reliable representation of the spike.

Clearly, some aspects of the stability and convergence of the EHL solution still need to be better understood, and so long as this remains true, computational schemes such as those of figure 4 cannot be run fully automatically. Indeed, the computations described herein were implemented in the interactive mode, allowing control to be steered between loops by changing weight factors or convergence criteria. It is, however, particularly encouraging in this respect to find that when different interactive routes for the same case were followed, an essentially path-independent solution was reached. Thus, progress toward the goal of an optimized convergence strategy (ref. 11), if slow, has been nonetheless positive.

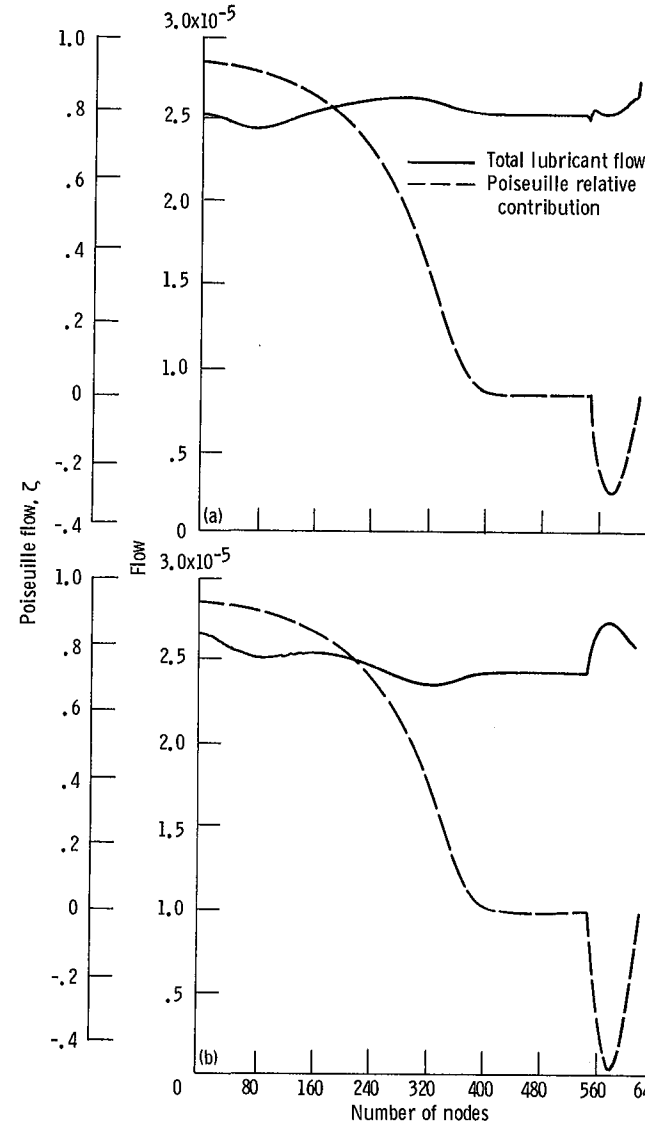

(a) Smooth boundaries.
(b) $\Lambda = 0.93$; $\gamma = 3$.

Figure 5.—Total lubricant flow and Poiseuille relative contribution.

Results and Discussion

Flow Effects

In guiding the computation through its final outer loops to convergence, the procedure was always terminated when the contact load agreed with the fixed input value to a part in 10^6 or better. The remaining test of convergence then is to examine flow variation through the contact, for which examples are provided in figure 5. For an effectively smooth surface (fig. 5(a)), where $\Lambda_{m,0}$ is larger than ~10, the constancy achieved for net flow was comparable with that exhibited in II under actual smooth-surface conditions. By contrast, for the smallest $\Lambda_{m,0}$ value (0.93) in the longitudinal case ($\gamma = 3$), figure 5(b) shows an increase in flow at the minimum film position due to incomplete balance between a reduced Couette term and an increase in the magnitude of the ζ (or Poiseuille term). Correspondingly, for isotropic asperities this irregularity is inverted as a result of a pronounced reduction in the magnitude of ζ.

According to equation (8) the Poiseuille term ζ reflects most strongly the variation of the pressure flow factor. Other factors in ζ are less sensitive to the roughness parameters. Data taken at the absolute minimum of figure 5 (minimum film thickness position) and normalized to the smooth value ζ_0 are presented in figure 6, which does indeed follow closely the pure flow factors of figure 2(a).

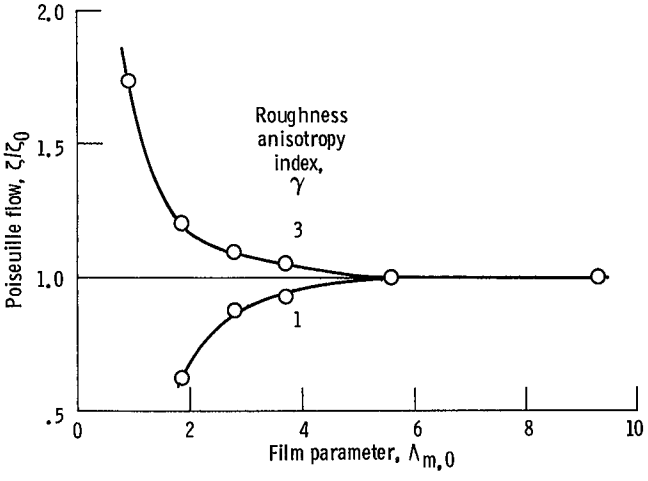

Figure 6.—Poiseuille flow term at minimum film thickness for rough surfaces (normalized to smooth-surface value $\zeta_0 = -0.277$).

Film Shape Effects

The pressure and film shape have been presented in figure 3 for the values of U, W, and G chosen. Since, as we noted earlier, roughness produces changes at the 1 percent level, figure 3 would not be perceptibly altered for any of the physically reasonable values of $\Lambda_{m,0}$ considered here. On a much enlarged scale values of the absolute minimum film thickness $H_m/H_{m,0}$ in the nip downstream from the pressure spike are shown in figure 7 as a function of $\Lambda_{m,0}$ for γ of 1 or 3. Values are normalized to the smooth-surface value, which was taken to be the mean of the two values at the largest $\Lambda_{m,0}$ considered, differing by only 3×10^{-3}. (This same normalization procedure was followed also in studying the variation of traction and flow.) The smooth curves joining the computed points have been sketched simply to aid visualization, and the scatter about the two lines gives an indication of the accuracy of the method. This is determined largely by the degree to which the converged

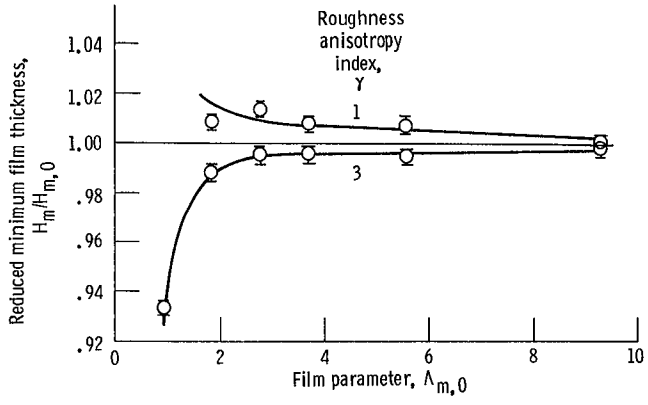

Figure 7.—Dependence of minimum film thickness at constant load on film parameter for different asperity anisotropy (normalized to smooth-surface value $H_{m,0} = 1.99\times10^{-5}$).

solution is independent of the iteration path followed. As $\Lambda_{m,0}$ becomes smaller, convergence is harder to achieve for any γ value. In particular, when $\Lambda<2$, $\varphi_{11}^{\rho*}$ becomes negative if $\Lambda^2<3(2-\gamma)/(1+\gamma)$, which has the value 1.22 for $\gamma=1$. The occurrence of negative flow factors near the minimum film thickness is an obvious indication that the limit of physical validity of the model has been surpassed.

The film shape shown in figure 3 displays two other extrema: a weak maximum upstream of the spike, and a very shallow minimum located a few nodes downstream of center. Data for these secondary extrema resemble quantitatively those for the absolute minimum of figure 7. This may be compared with the results of Patir and Cheng (ref. 12), who performed a calculation on the inlet half only of a line contact to determine the effect of their flow factors on central film thickness. In qualitative agreement with figure 7, results for $\gamma<2$ curve upward and vice versa, but in the isotropic case, for which quantitative comparison is possible, the slope of their curve is about 10 times greater than ours. This difference could well be attributed to the Grubin-like approximation to the inlet shape, details of which are known to have a large influence on the pressure buildup.

Pressure Effects

A discussion of pressure spike behavior has been foreshadowed in the preceding section. Fractional changes in the central pressure maximum and in the minimum preceding the spike were somewhat smaller than the changes found in the secondary features of the film shape. For the most part then, P was even less sensitive to roughness than H. Clearly, if changes in spike height due to roughness also fell below 1 percent, the present technique could not reliably estimate the effect. All but two of the cases run so far were consistent with a spike of constant height and shape that simply moves a few tenths of a grid spacing upstream for longitudinal roughness or remains essentially stationary for the isotropic case. Only for the extreme $\Lambda_{m,0}$ values did a fixed shape fail to fit. In the longitudinal case the height appeared to drop by about 5 percent for $\Lambda_{m,0}\sim1$, while an increase of similar magnitude occurred for isotropic asperities, $\Lambda_{m,0}\sim2$. Although these values lie outside the physical regime for which the model is valid, the mathematical continuation is smooth, and the results are indicative of trends too small to observe in the physical range. Even so, the conclusion with respect to spike height advanced here depends on the assumed shape and remains subject to verification at finer grid sizes.

Traction Effects

Results of the traction coefficient calculations based on equation (21) have been plotted in figure 8 using the same

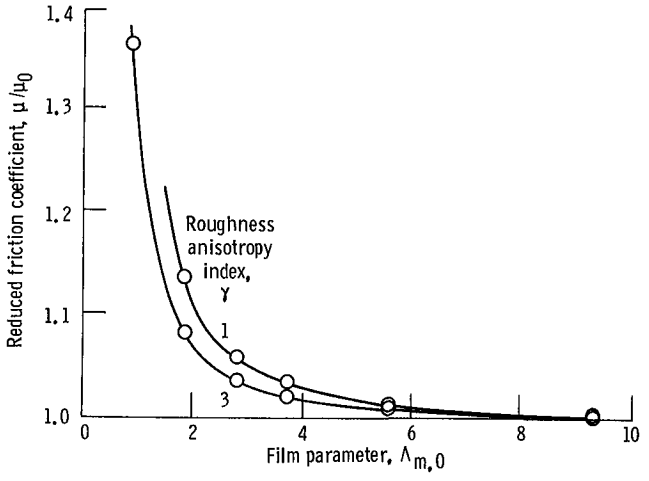

Figure 8.—Dependence of friction coefficient on film parameter (normalized to smooth-surface value $\mu_0 = 5.51 \times 10^{-4}$).

format as the previous figure. A significant difference between the two diagrams, both normalized to smooth values, is the general scale of the effect, which for traction showed changes of about 5 percent in the full-film range, $\Lambda_{m,0} > 3$, increasing to over 10 percent as $\Lambda_{m,0}$ decreased to 2 in the partial lubrication regime. A further important distinction is that roughness increased traction for both isotropic and longitudinal asperities, and hence by extension for all γ values, whereas the other effects discussed in this work each changed sign at the critical $\gamma = 2$ value. The large magnitude of the relative increase can be understood by examining equation (18), which shows that traction arises from the loss of x symmetry of the film shape and pressure distributions as a result of both elastic and hydrodynamic effects—a film with a symmetric (e.g., Hertzian) pressure field would be frictionless. The influence of roughness, though small on H or P individually, has a large effect on the detailed balance of the positive and negative contributions to μ, given the actual unsymmetrical H and P distributions. It turned out in agreement with intuition that isotropic or transverse roughness produced the larger increase in μ. In the work of Bush et al. (ref. 13) on a lightly loaded point contact, friction increases for all γ values, but in contrast, longitudinal textures show the larger effect. This difference in ordering with respect to γ seems to be associated with the absence of side leakage in line contact. However, with traction in the pure rolling case appearing only as a result of the departure of H and P from perfect symmetry, the γ dependence in different dimensions is difficult to predict.

Conclusion and Outlook

We have set up a formal method for incorporating the effects of roughness on lubricant films and have applied the model to the detailed computation of film shape and pressure distribution in an elastohydrodynamically lubricated (EHL) line contact. The many assumptions of the procedure have been discussed and include the following: First, roughness should be of the Reynolds type, which requires long wavelengths and small amplitudes for the asperities relative to film thickness. Under these conditions the flow factor modification of Reynolds hydrodynamics and the perturbation evaluation of these flow factors are both valid. Average flow has been aligned with a roughness axis, a condition occurring in practice in many finishing processes for rollers, where the lay is circumferential. By making use of the complete flow factor tensor, this condition can be relaxed to handle cases where special textures are imposed to achieve net transverse flow. Finally, the selection of operating parameters assigned the contact to the piezoviscous-elastic regime. Specifically, we have taken an incompressible, isothermal Newtonian fluid with Roelands viscosity entrained by two cylinders in pure rolling. Since the shear flow factors are also known from equation (3), an obvious extension of these computations would be to relax this last condition to include slip effects.

With these basic assumptions detailed results were obtained for a range of film parameters $\Lambda_{m,0}$ corresponding to surface roughness amplitudes from 0.1 to 1.0 times the smooth-surface minimum film thickness. Anisotropy effects were included by studying both isotropic asperities ($\gamma = 1$) and asperities three times longer on average in the flow direction than transverse to it ($\gamma = 3$).

A significant conclusion of this work is the weakness of the influence of roughness on both film shape and pressure distribution. In the physically valid regime of $\Lambda_{m,0}$, greater than at least 2, the identifiable extrema of both changed fractionally by 1 percent or less. For longitudinal asperities both film thickness and pressure were reduced, with opposite changes for isotropic and transverse roughness. Although the two γ values used in this study served to indicate the general magnitude of the effect, it will be worthwhile to examine the γ dependence more fully, especially since there exist so many other treatments with which to compare the limiting one-dimensional roughness cases, where γ is either 0 or ∞. From the pressure flow factors it seems clear that the

magnitude of roughness effects should increase as either of these extrema is approached.

Although it might be anticipated that the height, at least, of the pressure spike would be sensitive to roughness details, the calculations again did not bear this out. Because of its extreme narrowness the grid size defined the spike with too few points, and some assumption about its shape was necessary. A fixed shape was consistent with the data, in which case the height was invariant with roughness to within the accuracy of the computation. For $\Lambda_{m,0}$ values at the extreme low end of the range a slight trend did emerge, suggesting that longitudinal asperities reduce the height and vice versa. This follows the same pattern established by the other extrema of P. Progress in understanding this behavior rests upon introducing a finer grid at least in the neighborhood of the spike.

In contrast with the insensitivity of averaged film shape and pressure to roughness, the behavior of the traction coefficient manifested increases greater by almost an order of magnitude in the same $\Lambda_{m,0}$ range. This may well be the most important practical consequence of the model developed in the present work. It suggests that surface roughness provides further variables, in addition to the usual fluid rheology parameters, that could usefully be manipulated to control traction in an optimal manner.

The present work was confined to the full-film lubrication regime and only hinted at effects that can be found in mixed lubrication. An evaluation of flow factors in this regime by Bush and Hughes shows that the largest effect of asperity contact occurs in the shear flow factor, suggesting that roughness effects should be sought in sliding situations. In addition, extension into the mixed regime requires a load compliance model for the asperities. No problems, in principle, block progress along these lines, but difficulties associated with numerical stability and convergence of such extended EHL computations will no doubt demand careful handling. The results will be of particular interest in the case of traction studies.

Lewis Research Center
National Aeronautics and Space Administration
Cleveland, Ohio, April 11, 1985

References

1. Hamrock, B.J.; and Dowson, D.: Ball Bearing Lubrication. Wiley, 1981.
2. Elrod, H.G.: A Review of Theories for the Fluid Dynamic Effects of Roughness on Laminar Lubrication Films. Surface Roughness Effects in Lubrication, D. Dowson, et al., eds., Mechanical Engineering Publications, London, 1978, pp. 11–26.
3. Elrod, H.G.: A General Theory for Laminar Lubrication with Reynolds Roughness. J. Lubr. Technol., vol. 101, no. 1, Jan. 1979, pp. 8–14.
4. Patir, N.; and Cheng, H.S.: An Average Flow Model for Determining Effects of Three-Dimensional Roughness on Partial Hydrodynamic Lubrication. J. Lubr. Technol., vol. 100, no. 1, Jan. 1978, pp. 12–17.
5. Tripp, J.H.: Surface Roughness Effects in Hydrodynamic Lubrication: The Flow Factor Method. J. Lubr. Technol., vol. 105, no. 3, July 1983, pp. 458–465.
6. Hamrock, B.J.; and Jacobson, B.O.: Elastohydrodynamic Lubrication of Line Contacts. ASLE Trans., vol. 27, no. 4, Oct. 1984, pp. 275–287.
7. Patir, N.; and Cheng, H.S.: Application of Average Flow Model to Lubrication Between Rough Sliding Surfaces. J. Lubr. Technol., vol. 101, no. 2, Apr. 1979, pp. 220–230.
8. Bush, A.W.; and Hughes, C.D.: The Average Flow Model: A Greens Function Approach. Proc. 10th Leeds-Lyon Symp. on Tribology, Lyon, 1983.
9. Weibull, W.: Glidlagerteori med Variabel Viskositet (Theory of Journal Bearings with Variable Viscosity). Teknisk Tidskrift (Mekanik), vol. 55, no. 51, Dec. 19, 1925, pp. 164–167.
10. Roelands, C.J.A.: Correlational Aspects of the Viscosity-Temperature-Pressure Relationship of Lubricating Oils. Ph.D. Thesis, Technische Hogeschool, Delft, Netherlands, 1966 (V.R.B. Groningen, pub., 1966).
11. Hamrock, B.J.; and Tripp, J.H.: Numerical Methods and Computers used in Elastohydrodynamic Lubrication. Proc. 10th Leeds-Lyon Symp. on Tribology, Lyon, 1983.
12. Patir, N.; and Cheng, H.S.: Effect of Surface Roughness Orientation on the Central Film Thickness in E.H.D. Contacts. Elastohydrodynamics and Related Topics, D. Dowson, et al., eds., Mechanical Engineering Publications, London, 1979, pp. 15–21.
13. Bush, A.W.; Skinner, P.H.; and Gibson, R.D.: Surface Roughness Effects in Point Contact Elastohydrodynamic Lubrication. Wear, vol. 83, no. 2, Dec. 15, 1982, pp. 285–301.

1. Report No.	2. Government Accession No.	3. Recipient's Catalog No.
NASA TP-2488		

4. Title and Subtitle	5. Report Date
Surface Roughness Effects in Elastohydrodynamic Contacts	July 1985
	6. Performing Organization Code: 505-33-12

7. Author(s)	8. Performing Organization Report No.
John H. Tripp and Bernard J. Hamrock	E-2524
	10. Work Unit No.

9. Performing Organization Name and Address	11. Contract or Grant No.
National Aeronautics and Space Administration Lewis Research Center Cleveland, Ohio 44135	13. Type of Report and Period Covered: Technical Paper

12. Sponsoring Agency Name and Address	14. Sponsoring Agency Code
National Aeronautics and Space Administration Washington, D.C. 20546	

15. Supplementary Notes

John H. Tripp, Case Western Reserve University, Cleveland, Ohio, and National Research Council - NASA Research Associate; Bernard J. Hamrock, Lewis Research Center. Presented at Eleventh Leeds-Lyon Symposium on Mixed Lubrication and Lubricated Wear, Leeds, England, Sept. 4-7, 1984.

16. Abstract

Theoretical studies of surface roughness effects in full-film EHL contacts are described. The analysis, using a flow factor modification to the Reynolds equation, was applied to piezoviscous-elastic line contacts. Carefully converged results for ensemble-averaged film shape, pressure distribution, and other mechanical quantities were obtained. Asperities elongated in the flow direction by a factor exceeding 2 decreased both film shape and pressure extrema at constant load; isotropic or transverse asperities increased these extrema. Changes were small, of order 1 percent, and the EHL spike showed no special sensitivity. The largest effects were displayed by traction, which increased by over 5 percent for isotropic or transverse asperities and by slightly less for longitudinal roughness.

17. Key Words (Suggested by Author(s))	18. Distribution Statement
Elastohydrodynamic lubrication Surface texture Nonconformal contacts	Unclassified - unlimited STAR Category 37

19. Security Classif. (of this report)	20. Security Classif. (of this page)	21. No. of pages	22. Price*
Unclassified	Unclassified	13	A02

*For sale by the National Technical Information Service, Springfield, Virginia 22161

NASA-Langley, 1985

National Aeronautics and
Space Administration

Washington, D.C.
20546

Official Business
Penalty for Private Use, $300

BULK RATE
POSTAGE & FEES PAID
NASA Washington, DC
Permit No. G-27

NASA

POSTMASTER: **If Undeliverable (Section 158 Postal Manual) Do Not Return**